

# 4D-Printing of Concrete via In-Situ Embedment of RFID Tags and Electronic Components for use in structural Health Monitoring.

William Makinen, *M.Eng, Mechanical and Aerospace Engineering*

**Abstract**—Structural health monitoring (SHM) of concrete infrastructure is essential for ensuring the continued performance and safety of these structures, which often have lifespans spanning decades. SHM can provide valuable insights into the condition of concrete infrastructure, allowing for timely repairs and maintenance to be carried out before more serious problems arise. Concrete additive manufacturing (AM) or 3D-printing (3DP) has seen a rise in popularity in recent years, with the potential to significantly reduce construction costs and speed up construction times, however there is little data on the long-term degradation of concrete 3D-printed structures. SHM of C3DP components can help bridge this gap, allowing for intermediate monitoring without having to characterize long-term performance before deployment. Passive wireless RFID moisture sensors embedded in concrete components have been shown to be a promising technique for cheap, reliable, and long-term structural health monitoring, however these sensors have never been integrated into a C3DP process. In this work, a novel process for automatically embedding RFID tags and other electronic components into concrete 3D-prints was developed to create a concrete 4D-printing process (C4DP). As opposed to traditional 3D-printing, 4DP involves the augmentation of 3DP components with self-sensing and self-actuating components to create active, smart materials. Here, the automatic embedment of sensors allowed for the creation of a smart, self-sensing concrete, with RFID tag signal attenuation characterized with respect to tag embedment depth. In addition, a pick-and-place system was developed for use as a general-purpose process for embedding arbitrary electronics into 3D-prints, allowing for any 3DP process to become “smart.” These systems were built upon a tool-changing 3D-printer, with their feasibility being successfully validated via the automatic placement of RFID tags within C3DP beam and the fabrication of polymer components with automatically embedded electronic components.

**Index Terms**—RFID, structural health monitoring, concrete 3d-printing, 4d-printing, automated manufacturing.

## I. INTRODUCTION

**S**TRUCTURAL health monitoring (SHM) of concrete infrastructure is critical to ensure continued performance and safety of structures throughout their lifespan, often spanning decades [1]. The importance of SHM has been brought into sharp focus recently, with events such as the 2021 Miami apartment building collapse resulting in loss of almost 100 lives [2]. This tragic event was caused in part by water damage to rebar and the surrounding concrete, and highlights the need for effective SHM to prevent such disasters in the future. Concrete is a widely used material in construction, and the maintenance and repair of concrete structures can be expensive and resource-intensive, often resulting in inadequate monitoring for less critical structures. SHM can provide valuable

insights into the condition of concrete infrastructure, allowing for timely repairs and maintenance to be carried out before more serious problems arise. Additionally, concrete additive manufacturing (AM) or concrete 3D-printing (C3DP) has seen a rapid increase in popularity in recent years [3], as it has the potential to significantly reduce construction costs and speed up construction times while allowing for additional structural complexity and automated processes [4]. While important for traditionally fabricated concrete structures, SHM is even more salient for concrete AM, as its novelty alongside its rapidly increasing use means that there is little time to perform long-term (years to decades) degradation studies on concrete AM structures before they are deployed for widespread, long-term use. SHM of C3DP components can help bridge this gap, allowing for intermediate monitoring without having to characterize long-term performance before deployment.

Studies with traditionally fabricated have shown that the moisture content of concrete is indicative of both its curing stage and strength as well as its long-term health and degradation [5], thus moisture or humidity sensors embedded into concrete components is a common SHM technique. However, most current implementations are wired or require the embedded sensors to be battery-powered. This significantly increases monitoring times and costs and limits the sensor placement flexibility and number of sensors that can feasibly deployed. SHM using passive, battery-free moisture sensors is a far more promising option [6], reducing measurement times and costs and increasing the potential number of senors that could be deployed.

Few efforts have been made to perform SHM of concrete using passive moisture or humidity sensors to date. Gong et al developed a piezoelectric backscattering system using mechanical waves within a concrete component to power up an embedded sensing node [7]. While impressive, this technique is less applicable to C3DP components due concrete AM’s layerwise material deposition process, which would disrupt and attenuate mechanical waves. Strangfeld et al developed a custom passive Radio Frequency Identification (RFID) [8] tag containing communication and moisture sensing circuitry that could be read wirelessly while embedded in concrete [9]. The tag’s performance was fully characterized as well [10], with a real-world, long-term SHM study lasting 1000 days also being carried out [11], proving the efficacy of passive RFID sensors as a long-term SHM solution. However, the RFID tags developed were fairly large, expensive, and hard to manufacture at scale, limiting deployment options.

This study builds upon previous works by taking advantage of new RFID tag technologies. Rather than having to develop a custom moisture-sensing RFID tag, companies such as SMARTRAC have developed off-the-self solutions [12] since the work of Stranfeld et al that are easy to use and compatible with most Ultra-high Frequency (UHF) Gen2 RFID readers. Using off-the-shelf tags, the focus could instead be shifted to integrating tag embedment into the 3D-printing process. This is something that has never been done, as to date, SHM sensors have only ever been manually inserted into conventionally cast concrete components.

Doing so expands the dimensionality of C3DP into 4D-printing. In 4DP involves the fabrication of "smart" materials that are able to respond to stimuli in their environment such as heat, light, magnetic fields, pH, or moisture [13]. It involves the careful design of both the material's composition and its deposition during the printing process to fabricate the final components. This stimuli response can consist of self-actuation such as folding [14] or self-sensing to provide useful environmental information [15]. More recently, multi-material 4D-printing has been explored to allow for multiple types of stimuli response [16] and for varied material composition throughout a component [17], as will be done here.

The primary contribution of this work is the development of a 4D-printing system for automatically embedding RFID tags and other components into a concrete 3D-prints using a tool-changing 3D-printing platform. It consisted of three parts: (1) the development of an RFID tag deposition tool for use with a tool-changing 3D-printer; (2) a characterization of RFID signal attenuation with respect to tag embedment depth; and (3) the development of a pick-and-place [18] tool to allow for arbitrary components to be embedded within a 4D-printed component. This work ultimately culminated in the successful automatic fabrication of a concrete beam containing an embedded RFID tag, and a demonstration of the feasibility of the pick-and-place system.

## II. DEVICE

The primary part of this research involved the development of an RFID tag deposition and pick-and-place tool for a desktop tool-changing 3D-printer. Both tools were then tuned and processing parameters were developed in accordance with the existing control scheme of the device as described in the following sections.

### A. Device Overview

The machine itself was built upon a commercial tool-changing 3D-printing platform and is detailed below with the primary components labeled in Figure 1.

The tool-changing 3D-printing platform is an E3D ToolChanger [19], and was obtained as an open-source kit consisting of the frame, motion system, and control electronics. The ToolChanger is easily modified and allows for a wide range of customizability, consisting of a movable tool mount (Fig. 1g) that uses a kinematic coupling mechanism to pick up and park up to four different tool heads. Although the kit shipped with four Hemera [20] polymer extrusion

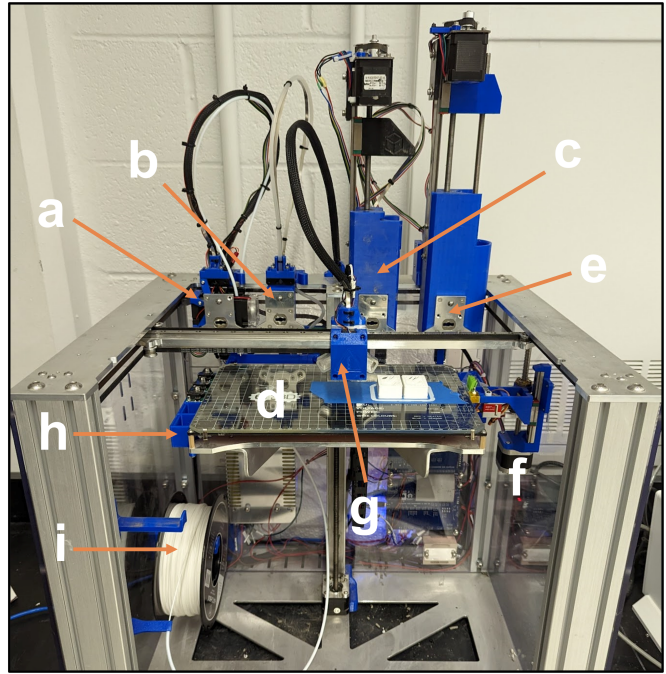


Fig. 1. The tool-changing 3D-printer: a. Hemera polymer extrusion tool b. RFID tag deposition/pick-and-place tool; c. concrete extrusion tool; d. build platform; e. tool plate; f. polymer extruder priming mechanism; g. movable tool mount; h. pick-and-place component holder; i. polymer material spool.

tools, these tools are easily exchanged for anything that can interface with the tool mount via a tool plate (Fig. 1e) and be parked onto the frame when not in use, as shown in the figure. For example, four different polymer extruders of varying nozzle sizes could be used to print different parts of a model at different scales, or additive and subtractive fabrication processes could be combined with the use of a CNC or laser cutter tool. In this case, three of the four tools are being used, a reservoir-based direct ink writing (DIW) tool head configured as a concrete extruder (Fig. 1c), the custom-developed RFID tag depositing and pick-and-place tools (Fig. 1b: due to requirements within the lab, the RFID deposition and pick-and-place tools could not both be mounted simultaneously, thus they were switched out of the second tool position as needed), and a Hemera polymer extrusion tool (Fig. 1a). Note that the material extruded during these experiments was mortar, as it contained only fine aggregates in the form of sand and did not contain any coarse aggregates, however concrete is used throughout this paper to ensure broader understanding. The final tool was configured for other experiments as required by other lab members. Finally, Fig. 1f shows the priming mechanism used when printing with the polymer extrusion tool.

This configuration facilitated the exchange between the concrete and polymer extrusion tools, and the RFID tag deposition and pick-and-place tools (this combination will be referred to as the *component placement tools*). When it was time to deposit a component into the print, the concrete or polymer extruder was parked and a component placement tool was picked up. After depositing the RFID tag or electronic component in the desired location, the extruding tool was then

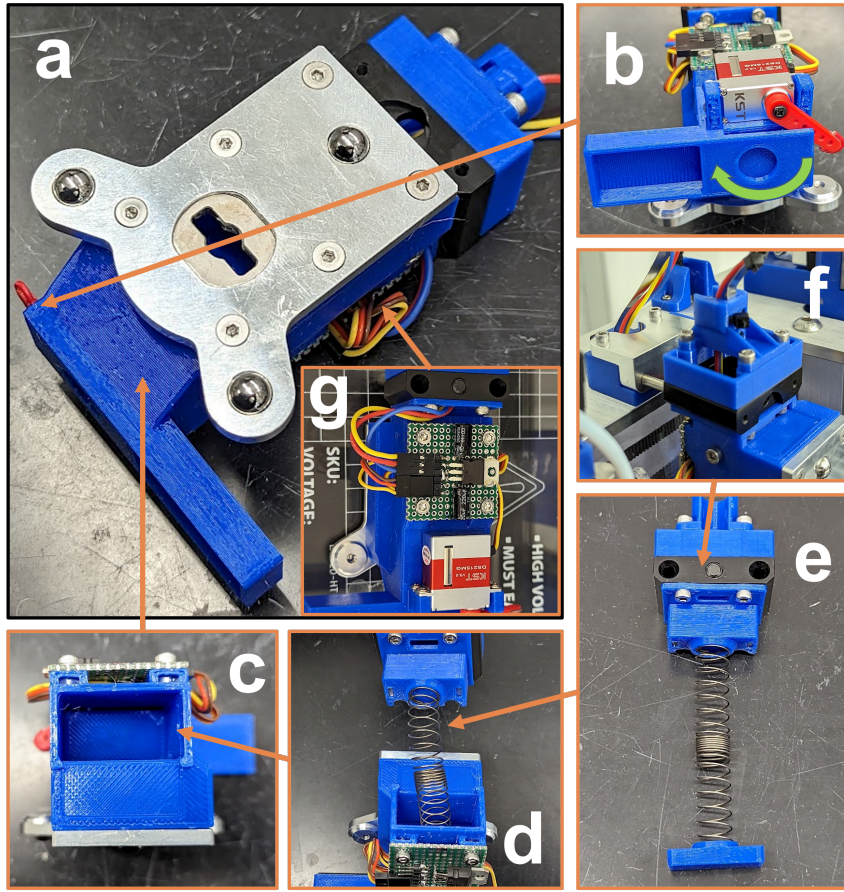


Fig. 2. The RFID tag deposition tool: a. tool overview showing the tool plate (silver); b. servo depositor mechanism and output slot; c. domino hopper; d. spring hold-down mechanism inserted into hopper; e. spring mechanism mounted to hopper lid; f. tool parked onto printer frame; g. integrated power regulation circuit.

switched back to and the rest of the print could continue.

#### B. RFID Tag Deposition Tool

The RFID tags used were the Gen2 UHF Higgs-EC adhesive tags [21]. As adhesive tags, they were paper-thin, and did not lend themselves well to robotic manipulation. Instead, they were adhered to 3D-printed "dominos," or extrusions with the same footprint as the adhesive tags but a much greater thickness. This was chosen to be 2.7mm, to match the chosen concrete printing layer height while being thicker than the servo's pushing arm (Fig. 3b) and allowing them to be pushed out of a hopper. This domino design is shown in Fig. 3.

The RFID tag deposition tool is shown in Fig. 2. Its primary components are the tool plate (Fig. 2a), the domino hopper (Fig. 2c), and the servo depositor (Fig. 2b). The tool plate interfaces with the kinematic coupling mechanism of the moveable tool mount (Fig. 2c) and allows the deposition tool to be moved about the build area. When not selected, the tool is parked using a slotting mechanism built into the device's frame as shown in Fig. 2f. The domino hopper is able to hold up to 12 RFID tag dominos at a time, and uses a spring mounted to the hopper lid (Fig. 2d and 2e) push the dominos towards the servo depositor while providing enough friction

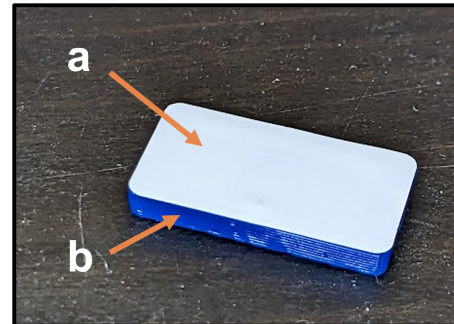


Fig. 3. An RFID tag domino used to facilitate RFID tag placement within prints: a. RFID tag sticker; b. 3D-printed extrusion.

to prevent the dominos from slipping out of the output slot until pushed by the servo arm. The servo depositor simply rotates its servo arm (red) 180°when commanded (illustrated by the green arrow in Fig. 2b) to force the bottom-most domino from the hopper through the output slot past the floor of the hopper, where gravity takes hold and the domino drops onto the desired location below the output slot. Finally, the servo has its own power regulation built into the tool, consisting of an LM7805 5v voltage regulator [22] and several decoupling

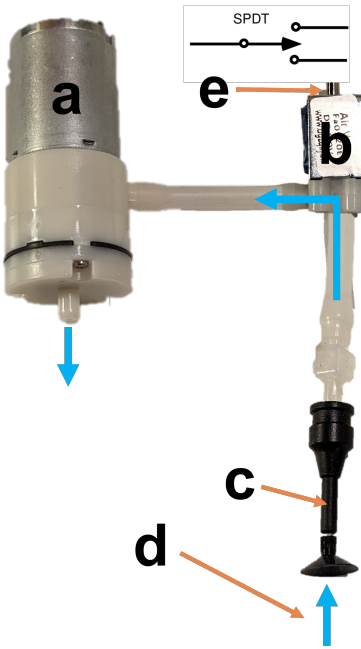


Fig. 4. A diagram of the pick-and-place system: a. suction pump; b. solenoid switch; c. suction cup end effector; d. suction force direction (blue arrows); e. solenoid switch exhaust port.

capacitors to convert the 24v from the device's built-in power supply to 5v usable by the servo (Fig. 2g).

Once complete, the RFID tag deposition tool was validated by precisely deposition six dominos in a row in a grid, using processing and toolpath design as described in section II-D2. It was able to do this multiple times without the hopper jamming or other errors occurring. A video of this can be seen at [23] (direct link).

### C. Pick-and-Place Tool

To enable true 4D-printing and the placement of arbitrary components within a print, a pick-and-place tool was constructed. It consisted of two primary components components: the suction tool itself and the component holder, as detailed in the following sections.

*1) Suction Tool:* The basic operating principles of the suction tool are shown in the diagram in Fig. 4. A suction pump (Fig. 4a) is responsible for creating a suction force (Fig. 4d, blue arrows) through a tube network ending in a suction cup end effector (Fig. 4c). The size of this suction cup and the power of the vacuum pump can be varied depending on the size and weight of the components to be placed. A single pole double throw (SPDT) solenoid switch (Fig. 4b) is responsible for switching the air flow between the suction cup end effector when carrying a component and an exhaust port (Fig. 4e) the rest of the time. This is necessary to immediately turn off the suction to the end effector when placing a part; the inertia of the suction motor results in some residual suction once the power is cut, impeding accurate placement by preventing parts from being released in a controlled manner.

The prototype realization of the pick-and-place tool is shown in Fig. 5. The suction pump and solenoid switch are

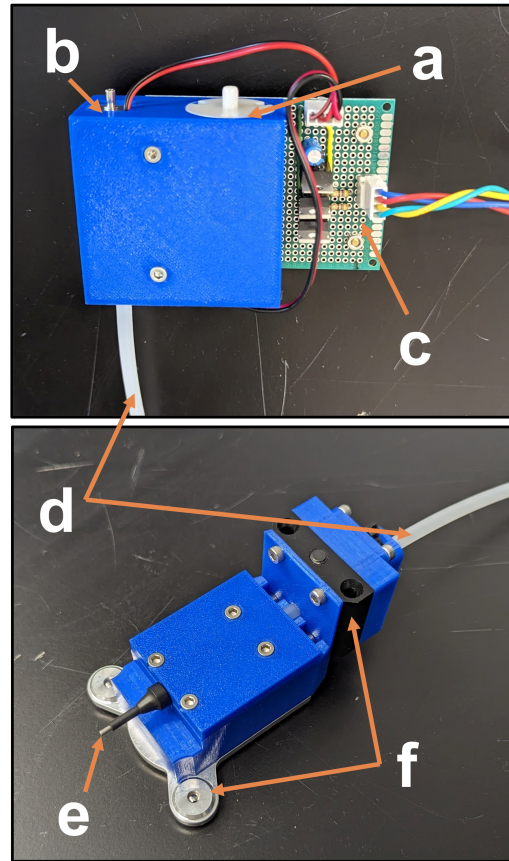


Fig. 5. Physical realization of the pick-and-place system: a. suction pump; b. solenoid switch; c. suction cup end effector; d. silicone tube from pump-switch system to end effector; e. control electronics.

contained in a 3D-printed housing (Fig. 5a and b) mounted to a control board with the control electronics (Fig. 5e). These electronics consists of the same LM7805 5v regulation circuit as the RFID tag deposition tool and two MOSFETs to modulate the pump and solenoid. The control board is mounted at the rear of the printer in the electronics housing area, while the suction end effector (Fig. 5e, shown here without a suction cup installed) is mounted to a tool plate and parking component (Fig. 5f) for interfacing with the toolchanging system, similar to the RFID tag deposition tool. Finally, the pump-solenoid system is connected to the suction cup end effector via a silicone tube run through the body of the printer (Fig. 5d).

*2) Component Holder:* To demonstrate the potential of a pick-and-place tool to be used in a 4D-printing system to print smart materials, a simple LED circuit was used as a representative payload for embedment. Shown in Fig. 6, it is a simple button-activated LED light that can be embedded in something such as a keychain. While simple, this is simply a demonstrative component. It could instead easily consist of any range of sensing or actuation electronics that could interface with the 3D-printed body of the component in any number of ways, such as by printing articulated structures [24].

A component holder was then fabricated to enable the loading of these electronic circuits. Shown in Fig. 7, it consists

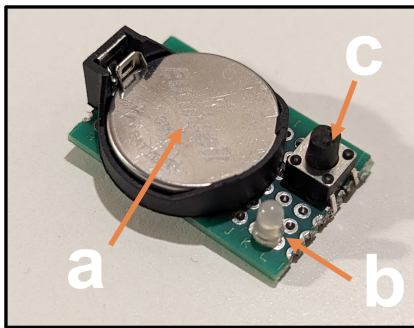


Fig. 6. The demonstrative LED circuit for embedment within 3D-prints: a. a coin cell battery power source; b. LED; c. momentary pushbutton.

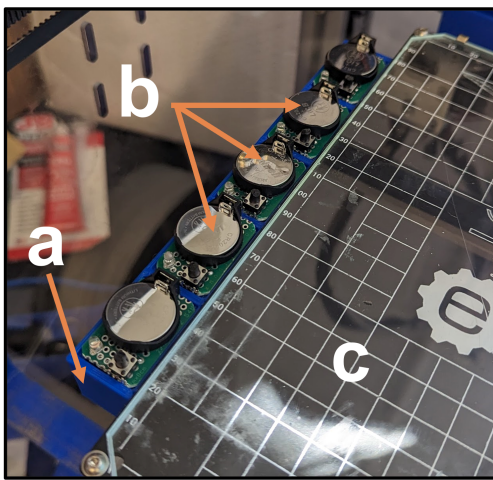


Fig. 7. The component holder used to hold the circuit components: a. 3D-printed holder; b. loaded LED circuits; c. z-axis mounted bed.

of a 3D-printed component (Fig. 7a) mounted to the z-axis controlled bed (Fig. 7c). This allows the components to be moved up and down, in and out of the range of the suction cup end effector. While designed to hold up to five of the LED circuits (Fig. 7b), it could easily be designed to hold any number of other components with simple geometry changes, and even multiple different types of components.

As a final note, while the RFID domino could have also been embedded using the pick-and-place tool, their regular, compact shape was more conducive to being densely packed in hopper system. On the other hand, the LED boards used to demonstrate the system were more irregular in shape and harder to package in a regular manner, and thus were more conducive using a holder system. This holder could easily be redesigned to hold other arbitrary components, with the potential to use a reel system in the future to serve more than five components at a time.

#### D. Device Control

The tool-changing device cannot function on its own. It requires firmware to control the hardware mechanisms and take in sensor inputs and control material extrusion, facilitate homing, and adjust other parameters in-situ to the 3D-

printing process. In addition, it requires software to generate the toolpaths that command the device to precisely extrude material in the desired patterns and deposit components in the proper locations. These modules are discussed in the following sections.

*1) Firmware:* The control electronics for the 3D-printer consist of a Duet 2 board, which uses a 32-bit microprocessor running RepRap Firmware (RRF) 3.0 [25]. RRF is an extremely powerful control paradigm for multi-tool 3D-printers, supporting a wide range of features not found in other 3D-printer firmwares. Typically, G-code commands are simply used to move a 3D-printer's tool to a specific XYZ-location at a particular feedrate, with M-codes being used to control auxiliary parameters, such as tool temperatures, fan speeds, accelerations, and the like [26]. In RRF, however, the G-code and M-code commands are more akin to a programming language. They can interface with deeper settings of the printer with the ability to change parameters that would typically have to be configured in a printer's firmware, such as configuring tool definitions and reading sensor inputs. Additionally, it is possible to run custom G-code macros, and use basic scripting features such as conditional statements and variable declarations within the G-code itself. Finally, the Duet 2 board is controlled through a built-in web interface running on the microprocessor itself, allowing the user to interact with the device over a network.

In this work, the scripting and variable features were used for priming the concrete extruder (necessary when switching back to it after having been parked, such as at the beginning of a print or after depositing an RFID tag), actuating the RFID deposition servo, and controlling the pick-and-place suction functions.

In order to ensure that the mortar was flowing evenly before starting a layer, a prime line of between 50-100 mm was first extruded. To save on print area, the prime line for a given layer was deposited on those before it, forming a vertical stack. However, priming only occurred after an RFID tag had been deposited, thus priming was not being performed on each layer, so the prime line could not be printed at the current z-height. Variables were used within a concrete priming macro to keep track of the number of primes that had been performed and the layer height of each extrusion. Thus, when it was time for another prime, the concrete extruder was able to move to the height required to print on top of the previous prime line. Macros were used to handle the servo positions for depositing an RFID tag and for facilitating tool changing as well.

G-code macros were also used to prime the polymer extrusion tool and keep track of the pick-and-place parameters. A counter was incremented each time a component was placed, indicating to the system to choose the next part from the holder. The G-code files for each part containing components also set system variables indicating the xyz-coordinates of each component, as well as when to initiate the pick-and-place sequence. Additionally, each component's G-code file contained details on the size and spacing of the components to be placed and the required suction pump strength.

2) *Toolpath Generation:* A tool called FullControl [27] was used to generate G-code toolpaths directly, bypassing the traditional 3D-modeling and slicing steps [28]. While the traditional pipeline works well for traditional 3D-printers, it is less well-suited to tool-changing, where it is necessary to precisely control extrusion parameters and facilitate tool-changing procedures. FullControl is a parametric tool that allows for the generation of rule and equation-based toolpaths rather than geometry-based ones, as is the case with 3D-modeling. In the context of this work, FullControl was used to create a beam generation design, where high-level parameters such as the beam's dimensions and the precise location of the RFID tag could be specified by the user without having to modify or re-slice a 3D model. A keychain toolpath with pick-and-place parameters and commands was also generated to demonstrate the pick-and-place functionality.

### III. EXPERIMENTAL SETUP

Experiments consisted of measuring the Received Signal Strength Indicator (RSSI) as reported by an off-the-shelf RFID reader of tags placed a constant distance away from the reader's antenna with varying thicknesses of concrete placed in between to simulate different RFID tag deposition depths. At each deposition depth, both C3DP and traditionally cast samples were tested to characterize the differences between each fabrication process. Additionally, each sample was tested 24 hours and 36 hours post-fabrication (it would have been beneficial to test at additional, longer time intervals however time limitations prevented such experiments) to analyze the effects of the concrete curing process (during which properties such as material density and moisture content change) on signal attenuation. In addition to measuring RSSI at each thickness, read time, or the time it took the reader to detect a tag after a search procedure was initiated, was also recorded. It was found to vary more predictably with changing material thickness than the RSSI measurements (the reader was relatively cheap and not the most sensitive), and is also a relevant metric to large-scale SHM applications. Should dozens or even hundreds of sensing RFID tags be placed in a building, they must be able to be found and read quickly by wireless readers, thus small time delays will add up substantially (this will become even more relevant should SHM scanning processes become automated).

As mentioned previously, obtaining the humidity-sensing RFID tags would have been ideal, as they would have allowed the moisture content of concrete components to be tracked over time as the cured. However, all mediums attenuate RF radiation depending on the material, its thickness, and density [29]. Thus, understanding the effect of deposition depth (as was done here) on the RFID signal attenuation in a given medium is necessary as it determines where within a component tags can be placed and the range of design flexibility possible. Finally, the maximum deposition depth tested was only 30mm due to the limited output power of the built-in PCB antenna of the RFID reader (27dBm), but the depths tested are still suitable to the desktop scale of the tool-changing 3D-printer and future experiments could use

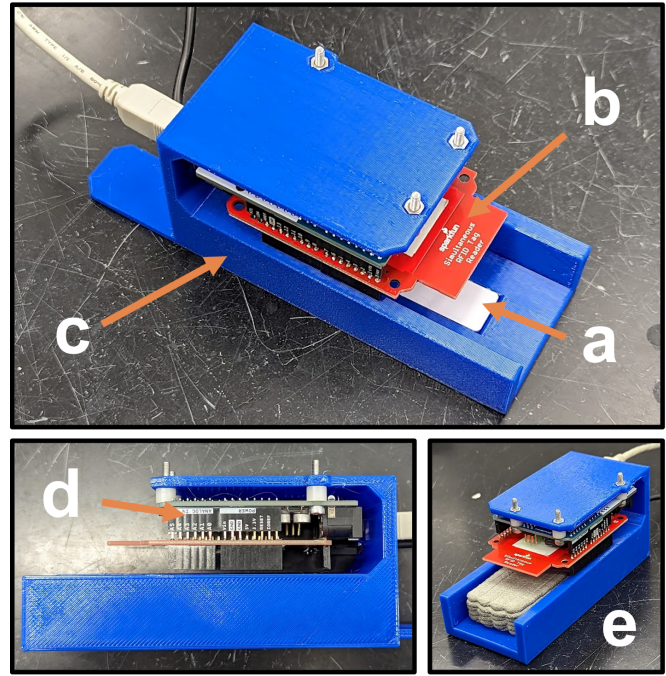


Fig. 8. The RFID tag testing rig: a. RFID tag domino placement at optimal read angle; b. RFID reader Arduino shield with integrated PCB antenna; c. 3D-printed frame with integrated clamp point; d. Arduino Uno microcontroller; e. test rig with concrete sample inserted.

more powerful readers/antennas to test deeper, more realistic deposition ranges.

#### A. Experimental Procedure

The test setup is shown in Fig. 8. The RFID reader is the ThingMagic Nano [30] with a maximum output power of 27 dBm mounted to an Arduino [31] shield with an integrated PCB antenna (Fig. 8b). Its frequency range was set to 917.4-927.2 MHz to comply with North American regulations and remain compatible with the UHF RFID tags. The data collection was performed by an Arduino Uno microcontroller board (Fig. 8d) connected to a Windows PC via a serial connection. A frame was 3D-printed (Fig. 8c) to hold the RFID reader's antenna a constant distance of 35mm (to accommodate the largest tested deposition depth) away from the RFID tag, which was placed with its domino into an integrated holding slot (Fig. 8a). A larger slot was also included to allow for the placement of C3DP and cast components of varying thicknesses to simulate different deposition depths (Fig. 8e).

A script was written for the Arduino to automatically collect measurements and report their averages and standard errors when commanded to by the user. 15 samples were taken at each material thickness for both fabrication type which were then further processed and plotted using a Python script. Because the reader was relatively low-cost and low-sensitivity, the reported RSSI values and read times often varied between measurements (on the order of several of dBm and tens of ms) even when reader and tag were held perfectly still. However, values stabilized and remained constant in aggregate (as seen by error bars on plots). Thus, each of the 15 samples



Fig. 9. A selection of the printed (bottom) and cast (top) samples tested.

were actually an average of 50 individual measurements, with averages and SEs taken across each set of 15 samples. During data collection, care was taken to clamp rig down and prevent perturbations, both mechanical and in terms of EMI, with area cleared of potential sources of interference. A selection of the printed and cast samples are shown in Fig. 9. Note the 3D-printed casing (blue) still seen around the edges of cast samples was left in place due to removal difficulty and its negligible impact on signal attenuation.

Samples were both 3D-printed and cast out of mortar using a sand as a fine aggregate, with the exact mix design shown in Table I. After fabrication, each sample was stored in a humidity chamber above 90% relative humidity to prevent cracking before being removed for testing after 24 hours, then kept in normal indoor conditions until 36 hours. The thickness of each C3DP sample was increased in units of layer heights, set to 2.7mm, with the molds of the cast samples being 3D-printed to match the final printed heights. The plots that will be seen in section IV-A use the final actual height of each sample as measured by calipers. 10 samples of each fabrication process were tested, varying from 1 layer in thickness to 10. The placement of the samples within the testing rig as seen in Fig. 8e was determined to be representative of full embedment, as within a concrete component there would be minimal multipaths and reflections from the surrounding material with only the material directly between the RFID tag and the reader being relevant to signal attenuation. This setup also facilitated easy switching between samples while using the same RFID tag for consistency.

TABLE I  
MORTAR MIX DESIGN

Component	Mass %
Cement Powder	54.7
Sand	27.3
Water	16.8
Gelanium 7700	0.48
VMA	0.65

In designing the RFID reader rig, the orientation of the RFID tags with respect to the antenna with the highest RSSI and lowest read time first had to be determined. This was to allow for the maximum range of testable concrete thicknesses

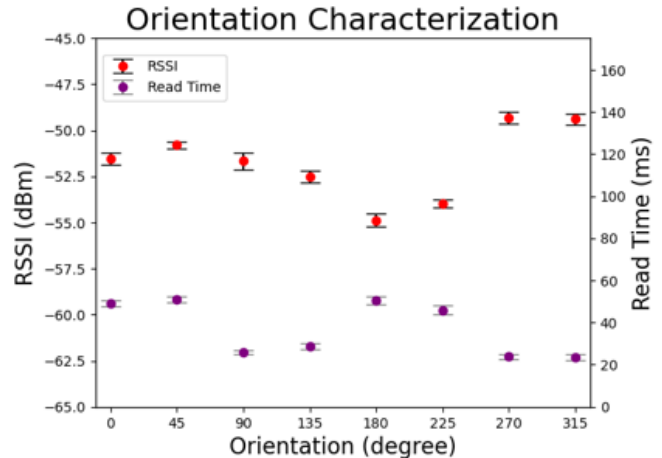


Fig. 10. RFID tag RSSI and sample time vs angle with respect to the RFID reader.

before there was a total loss of connection with RFID tags, especially given the limited output power of the reader. First, it was found that facing the tags face-up, parallel to reader was optimal (as opposed to being face-down or rotated 90°). From there, it was necessary to determine yaw angle with the best read properties. This was done by placing an RFID tag in the testing rig and measuring the RSSI and read time at various angle increasing in 45 degree increments. The results are shown in Fig. 10, with 270°relative to the reader having the best performance. Thus, the rig was designed to accommodate the placement of an RFID tag domino at 270°.

Finally, note that the units of the RSSI figures are the decibel ratio of the RSSI as reported by the reader in dBm to its set output power of 27dBm, and the error bars shown represent a 95% confidence interval

After the characterization had been performed, a full integration test was carried out. Serving as a proof-of-concept validation, this final test had the device fully fabricate a C3DP beam with an embedded RFID tag which was then successfully read after the beam had cured.

#### IV. RESULTS AND DISCUSSION

The following sections describe the results of the RFID signal attenuation experiments that were performed and the proof-of-concept RFID C3DP and pick-and-place component embedment process that was developed.

##### A. Signal Attenuation Characterization

The first test conducted measured the change the RSSI and read times with respect to sample thickness across each process 24 and 26 hours after fabrication, as shown in Fig. 11. Note that the dotted lines and red shaded areas indicate the thicknesses at which the reader could no longer detect the RFID tag at all. Interestingly, material thickness seems to have little effect on signal attenuation for the 3D-printed samples at 24 hours (Fig. 11a and 11b), with high thicknesses of over 20mm being necessary to observe any significant losses. For the printed samples, this is due to the curing

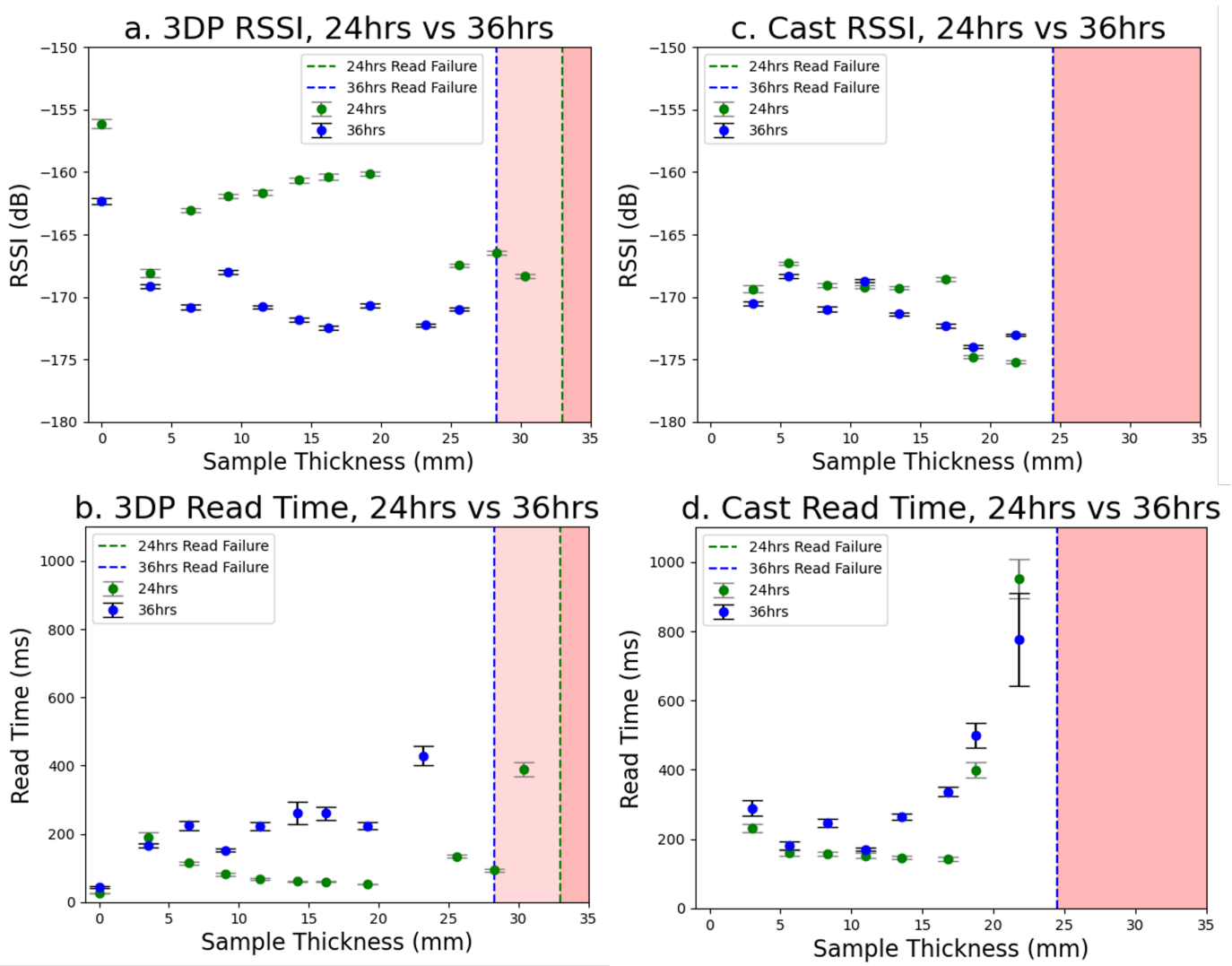


Fig. 11. Comparisons of signal attenuation at 24 and 36 hours after sample fabrication: a. 3DP RSSI; b. 3DP read time; c. cast RSSI; d. cast read time.

process of concrete. RF signal attenuation is directly correlated with material density [29]. Additionally, density is known to increase as concrete cures [32]. Thus, at 24 hours, less curing has occurred and all the samples are at a relatively low density, with results differing little to if there was no concrete in between the reader and tag at all. The exception is with the thinnest 1 or 2 layer samples, which initially appear to be anomalies. Part of the curing process is both absorption of water into the concrete materials and evaporation of water content from volume of component through component surfaces [33]. Smaller samples have a higher surface area to volume ratio, thus a higher percentage of their water is able to escape sooner, curing and densifying the component more quickly than thicker components. This resulted in the thinner samples attenuating RF more than the thicker ones at 24 hours, as they were at a further stage of curing, thus denser. By 36 hours, more curing had occurred across all the samples, producing a more predictable trend of increased signal attenuation with additional layers of 3DP concrete.

For the cast samples, this trend is less noticeable (Fig.

11c and 11d). This is due to the higher density of material distribution within the cast samples; the mortar material itself is of same density, however air gaps exist between the extruded filaments of the printed samples (also known as material deposition density). This allows the printed samples to cure more quickly, with a more noticeable change in signal attenuation at 36 hours compared to the cast samples with less surface area exposed to the environment. Thus, the cast samples remain more static, with only slight changes in RSSI and read time from 24 to 36 hours.

Next, signal attenuation was compared across fabrication techniques at 24 and 36 hours. As expected, the cast samples attenuated the RFID signal more, especially at the 24 hour mark (Fig. 12a and 12b) due to their higher material deposition density. This resulted in a higher volume of material in between the reader and tag given the same thickness of concrete, thus more attenuation occurred. (there is more matter in between the reader and tag, thus the signal is more likely to be absorbed, scattered, or reflected by impinging material). These air gaps present within the printed samples can be tuned

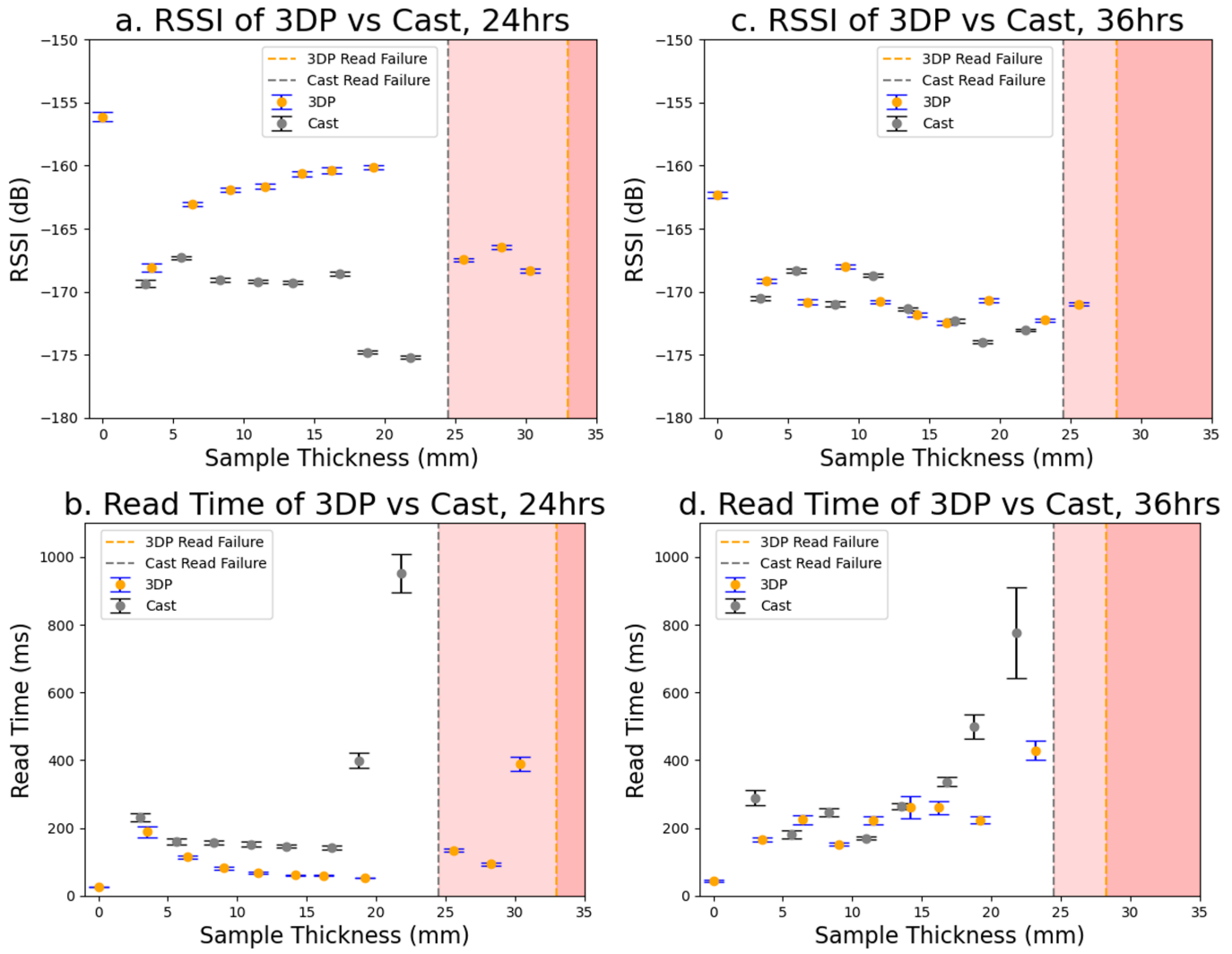


Fig. 12. Comparisons of signal attenuation at across the 3DP and casting fabrication processes: a. RSSI at 24 hours after fabrication; b. read time at 24 hours; c. RSSI at 36 hours; d. read time at 36 hours.

by varying the printing parameters, with similar densities and thus signal attenuation to cast components being achievable. However, the C3DP process provides additional flexibility and design options. A component may need to primarily consist of a higher density of concrete due to strength requirements, which may limit the placement of a tag to certain shallower, less desirable depths. But, by varying the density of the 3D-printed filaments in certain sections between the tag and reader locations, much more placement flexibility can be achieved without requiring significant tag placement or component strength compromises.

Note also that due to the lower surface area to volume ratio and slower curing of the cast samples, the printed samples are able to "catch up" to them in terms of signal attenuation effects by the 36 hour mark (Fig. 12c and 12d). While the cast samples remain relatively static, the printed samples increase in density significantly after 24 hours, allowing them to achieve similar RSSI attenuation and read time increases at a given thickness despite having much lower material deposition density.

A final note is that it may be possible to measure concrete curing and health simply using the RSSI measurements between a reader and a "dumb" tag, without any moisture or humidity sensing. Assuming a known distance between the reader and the tag, a known concrete thickness or embedment depth, a known reader signal strength, known attenuation properties of the specific concrete in question, and calibration between the three parts, a conversion function between RSSI and the concrete's density and moisture content could be derived. This would be hugely consequential, as sensorless RFID tags are much cheaper and more commonplace than those with built-in sensors. This would potentially accelerate the deployment of passive, wireless, RFID-based SHM systems, as they would be much cheaper and could be done with arbitrary tags assuming proper calibration.

#### B. Automatic RFID Tag Placement

Much of this work was dedicated to developing the RFID tag deposition tool and its associated toolpath and processing to allow for concrete 4D-printing. Full control and RRF3 used

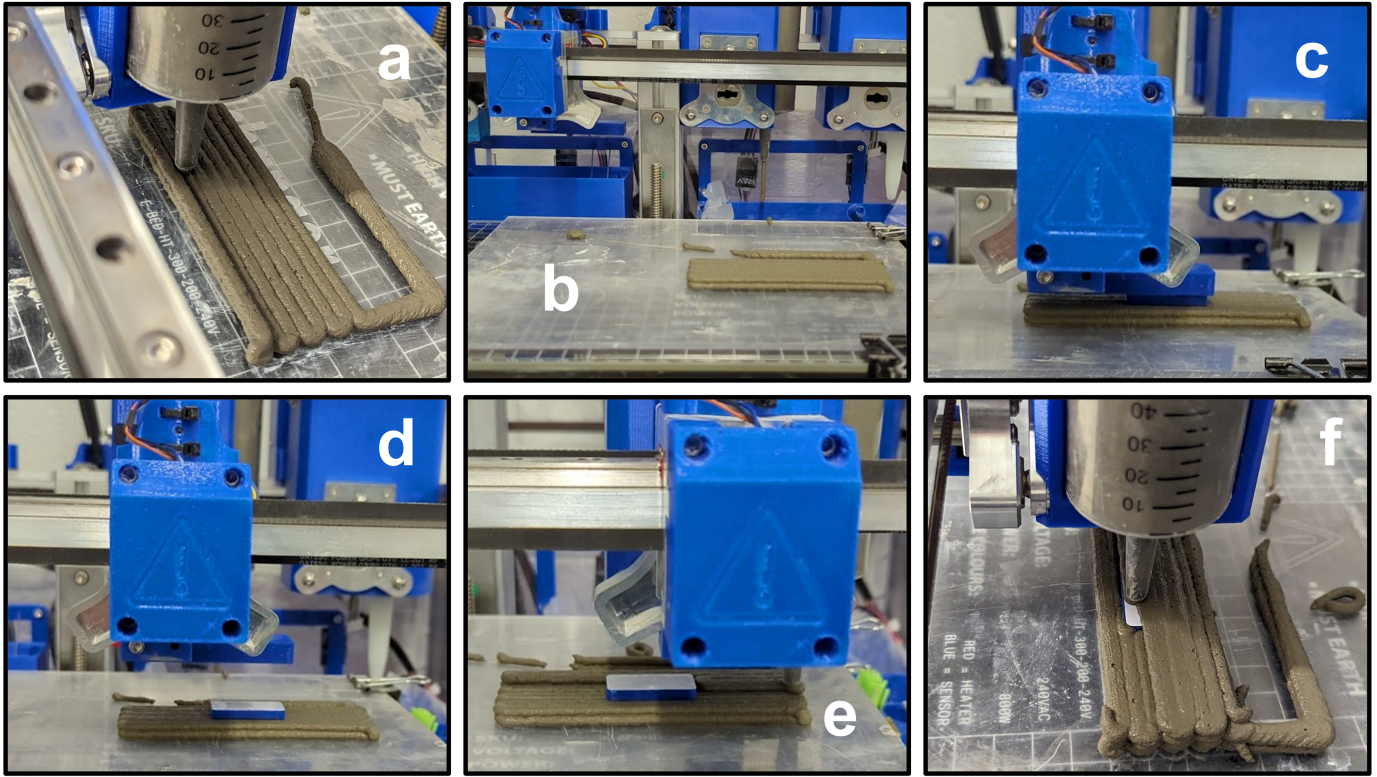


Fig. 13. A timeline of the RFID embedment process into a C3DP beam: a. initial layers printed; b. RFID tag deposition tool selected when RFID tag domino layer is reached; c. RFID domino is placed in specified location; d. deposition tool moves up out of the way; e. concrete extrusion tool is re-selected and prints around RFID tag; f. RFID tag is fully encased in concrete. Video at [23] (direct link).

to design the toolpath resulting in the printing process shown in Fig. 13 to fabricate a beam component with an embedded RFID tag. While it only prints a simple beam, its parameters are fully customizable via FullControl, including its outer dimensions, the placement of the RFID tag within the volume of the beam, as well as the tag’s embedment depth. For this proof-of-concept demo, a 100mm x 32mm beam was printed consisting of five 2.7mm layers, with the RDIF tag domino deposited on the third layer, two layers from either of the beam’s surfaces.

The initial layers are printed normally before the RFID tag layer is reached (Fig. 13a). Then, once the tag layer is reached, the concrete extruder is parked and the domino deposition tool is picked up (Fig. 13b). After moving over the chosen tag location, the domino deposition tool actuates its servo motor, pushing the RFID tag domino at the bottom of the hopper out into position (Fig. 13c and Fig. 13d). Finally, the tools are exchanged again the the concrete tool is used to print around and on top of the RFID tag domino (Fig. 13e and Fig. 13f), fully encasing it in concrete. The final result is shown in Fig. 14, and is indistinguishable from a uniformly concrete beam.

After curing, the embedded RFID tag was able to be read with similar performance as the 2-layer sample tested in section IV-A. This indicated that the testing methodology used was valid, and that the RFID tags obtained were sufficiently moisture resistant to be embedded in concrete. Overall, this test was a success, with RFID tag dominos reliably and precisely deposited in prescribed locations within a C3DP



Fig. 14. The completed C3DP beam with an embedded RFID tag.

component over multiple repetitions. A video of this process in action can be seen at [23] (direct link).

### C. Automatic RFID Tag Placement

To further expand the 4D-printing capabilities of this system, a pick-and-place tool was also developed. To demonstrate the feasibility of 4D-printing smart components with a tool-changing 3D-printer, a simple light-up keychain was fabricated. Shown in Fig. 16, it contains the LED circuit described in section II-C2. A thinly-printed flexible top layer allows for the pushbutton to be actuated, turning on the LED. Traditionally, a component such as this would have to be printed in at least two parts, with the electronics manually inserted and the use of fasteners likely. Instead, a single smart component, responsive to external stimuli, is 4D-printed in a single go with no manual intervention required. Note that

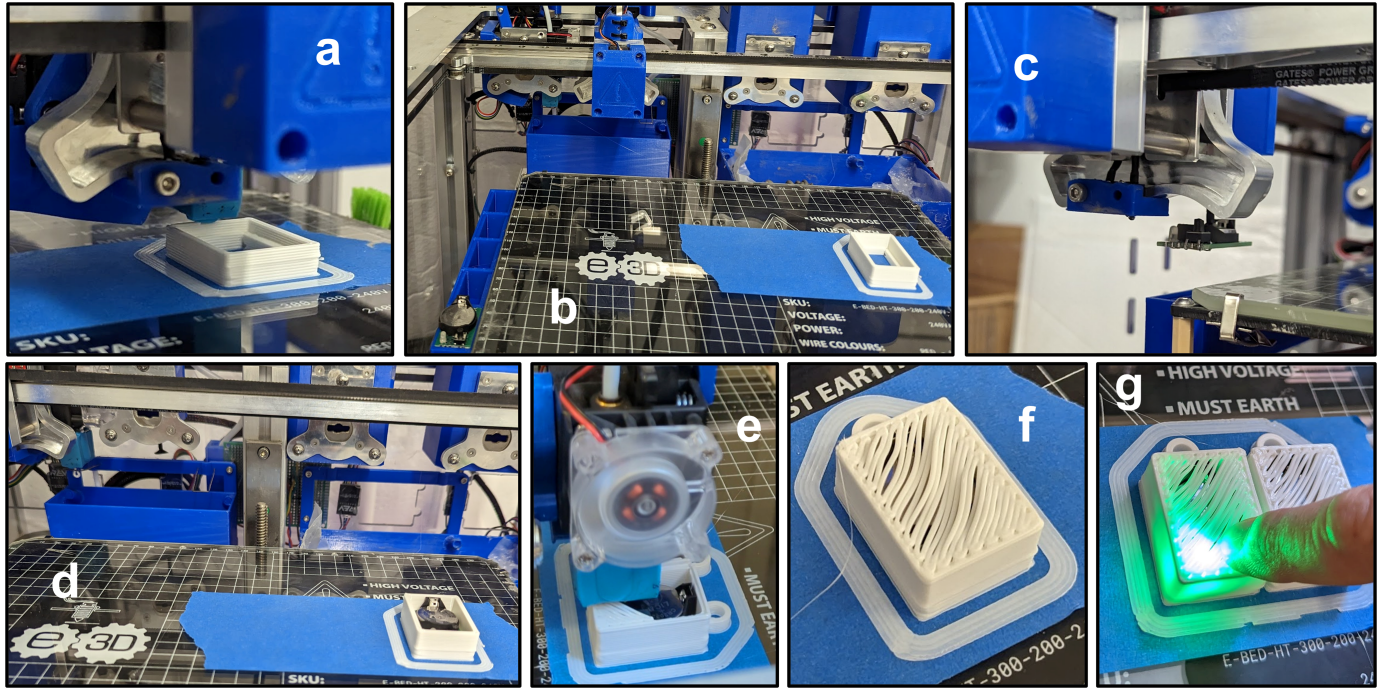


Fig. 15. A timeline of the pick-and-place process: a. component body printed; b. pick-and-place tool selected when triggered by macro; c. LED circuit is picked from holder; d. LED circuit is placed in component body; e. polymer extrusion tool is re-selected and seals in LED circuit; f. LED circuit is fully encased by component body; g. two keychains printed simultaneously. Video at [23] (direct link).

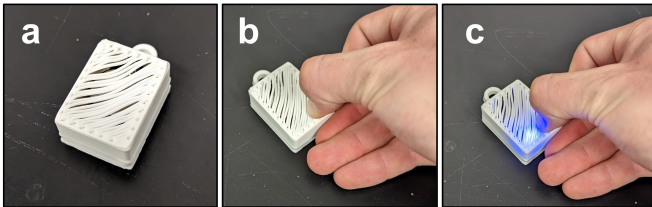


Fig. 16. The finished 4D-printed keychain: a. finished component; b. light off; c. light actuated via flexible top layer.

it was printed in polymer instead of concrete to show the flexibility of a pick-and-place 4D-printing system and for more rapid iteration during development and testing.

Shown in Fig. 15 is the fabrication process for this demonstrative keychain component. First, the body of the component is printed in a standard manner (Fig. 15a). Then, when triggered by a macro embedded in the G-code, the polymer extrusion tool is exchanged for the pick-and-place tool (Fig. 15b). The pick-and-place tool picks the LED circuit from the holder (Fig. 15c) by turning on the vacuum pump and activating the solenoid switch, lifting the part and placing it in the correct location within the 3D-printed body (Fig. 15d). The polymer extrusion head is then switched back to and the flexible top layer is printed (Fig. 15e), sealing in the LED circuit board and forming a single component with embedded electronics. This validated by printing a single keychain at a time (Fig. 15f) and by printing two at a time (Fig. 15g), demonstrating the usefulness of this 4D-printing system for smaller-scale manufacturing as well.

## V. CONCLUSION

In this work, a 4D-printing system for automatically embedding RFID tags within a C3DP component was developed using a tool-changing 3D-printer. A toolhead capable of depositing RFID tag dominos was designed, built, and demonstrated to work reliably, both in more limited validation tests and in carrying out the entire automated fabrication of an RFID-tag-embedded concrete beam. Additionally, characterization was carried out to determine how the embedment depth would attenuate the RFID reader's received signal. It was found that the relationship between concrete thickness and RSSI and read time is much more complicated than initially expected, and is dependent on other factors such as the material deposition density and curing stage of the concrete. While the desired humidity monitoring RFID tags were unable to be obtained, this characterization work is still relevant, as understanding how much concrete can be in between the tags and reader will be required for any tag embedment system. This research applies broadly to the fields of SHM and C3DP, and is the first known work to fully automate both the concrete manufacturing and sensor placement processes.

This concept was then generalized by developing a pick-and-place tool capable of placing arbitrary components such as electronics within concrete prints and those with other materials. This expansion allowed the toolchanging system to truly become capable of 4D-printing with the capabilities only limited by the materials available and the design skills of the user.

Moving forward, there are a number of potential avenues to explore to further progress this research. First, the humidity-sensing RFID tags would need to be obtained with these

experiments repeated by embedding them into both wet 3DP concrete and cast concrete. Signal attenuation vs embedment depth could still be measured, with it also being possible to monitor moisture content over 7-day and 28-day periods as is customary in concrete testing industry (the curing and hardening process never stops, however 28 days is generally considered fully cured and 7 days often used experimentally to speed up testing process [34]. These measurements could then be correlated to strength and curing properties by carrying out compressive strength tests. There is also the potential for determining an RSSI vs density formulation as described previously, which could be augmented with moisture level measurements.

Additionally, it would be useful to obtain more powerful RFID reader to test deeper and more realistic embedment depths that would be more practical for full-scale concrete components. This would also enable the scaling up of the tag-embedded components past the desktop scale, as larger concrete 3D-printers could be used to achieve deeper embedments. Finally, it would depend on the component geometry and size, but developing an automatic scanning process would also be an interesting endeavor to pursue as a way to fully robotize the process from fabricating to post-process monitoring. This would also require characterizing the effect of the concrete's thickness on the maximum speed the reader can move at and still detect tags, likely a related phenomenon to the increases in read time observed in this work.

The pick-and-place system could also be improved upon in a number of ways, primarily by adding closed-loop feedback. Industrial pick-and-place systems such as those used in circuit board manufacturing utilize complex computer feedback systems to ensure proper part orientation as well as pressure sensors to verify that components have actually been picked up [35]. Additionally, the suction cup end effectors feature a rotational degree of freedom, meaning that the orientation in the component holder does not need to match the final orientation once placed. Component-level pick-and-place could also be implemented, allowing for the electronic circuits themselves to be assembled in-situ rather than having to be pre-assembled. And, as mentioned previously, a number of other sensing circuits could be explored, with those that do not need to be powered by an internal battery being of particular interest (the fully-embedded, seamless nature of the final 4DP components does not lend itself well to easy battery exchange).

As a final note, concrete components with embedded RFID tags could be useful in a number of other contexts, even without moisture sensors. They could be used for component identification, which could be useful in construction applications where components are fabricated separately and then assembled on-site. The higher range of UHF Gen2 tags (up to 6 meters) could enable more flexible scanning options where vision-based barcode methods fail, or in cases where environmental exposure risks degrading externally-placed identification markers. Reader power and tag deposition depth could also be specifically chosen so that the tag sensing range remains small, allowing tags to serve as localization fiducials for robotic and other systems. This system could inform devices of the room they are in within a structure,

where the nearest exits are, and so on.

## REFERENCES

- [1] Sergej Johann, Christoph Strangfeld, Maximilian Müller, Björn Mieller, and Matthias Bartholmai. RFID sensor systems embedded in concrete – requirements for long-term operation. *Materials Today: Proceedings*, 4(5):5827–5832, 2017.
- [2] Randall W. Parkinson. Speculation on the role of sea-level rise in the tragic collapse of the surfside condominium (miami beach, florida u.s.a.) was a bellwether moment for coastal zone management practitioners. *Ocean & Coastal Management*, 215:105968, December 2021.
- [3] Yi Wei Daniel Tay, Biranchi Panda, Suvash Chandra Paul, Nisar Ahamed Noor Mohamed, Ming Jen Tan, and Kah Fai Leong. 3d printing trends in building and construction industry: a review. *Virtual and Physical Prototyping*, 12(3):261–276, May 2017.
- [4] Mohamadreza Moini, Jan Olek, Jeffrey P. Youngblood, Bryan Magee, and Pablo D. Zavattieri. Additive manufacturing and performance of architected cement-based materials. *Advanced Materials*, 30(43):1802123, August 2018.
- [5] Sanjeev Kumar Verma, Sudhir Singh Bhaduria, and Saleem Akhtar. Review of nondestructive testing methods for condition monitoring of concrete structures. *Journal of Construction Engineering*, 2013:1–11, April 2013.
- [6] Syed Humair Ali, Muhammad Zaid, Murad Abdullah, and Tariq Mairaj Rasool Khan. Shm of concrete bridge structures using wireless sensor networks, 2018.
- [7] Zheng Gong, Lubing Han, Zhenlin An, Lei Yang, Siqi Ding, and Yu Xiang. Empowering smart buildings with self-sensing concrete for structural health monitoring. In *Proceedings of the ACM SIGCOMM 2022 Conference*. ACM, August 2022.
- [8] Zhaozong Meng and Zhen Li. RFID tag as a sensor - a review on the innovative designs and applications. *Measurement Science Review*, 16(6):305–315, December 2016.
- [9] C. Strangfeld, S. Johann, M. Muller, and M. Bartholmai. Embedded passive RFID-based sensors for moisture monitoring in concrete. In *2017 IEEE SENSORS*. IEEE, October 2017.
- [10] M. Bartholmai, S. Johann, M. Kammermeier, M. Mueller, and C. Strangfeld. Transmission characteristics of RFID sensor systems embedded in concrete. In *2016 IEEE SENSORS*. IEEE, October 2016.
- [11] Christoph Strangfeld, Sergej Johann, and Matthias Bartholmai. Smart RFID sensors embedded in building structures for early damage detection and long-term monitoring. *Sensors*, 19(24):5514, December 2019.
- [12] atlasRFIDstore. Smartrac sensor patch rfid wet inlay, 2022.
- [13] Zia Ullah Arif, Muhammad Yasir Khalid, Ali Zolfagharian, and Mahdi Bodaghi. 4d bioprinting of smart polymers for biomedical applications: recent progress, challenges, and future perspectives. *Reactive and Functional Polymers*, 179:105374, October 2022.
- [14] Ali Zolfagharian, Akif Kaynak, Sui Yang Khoo, and Abbas Kouzani. Pattern-driven 4d printing. *Sensors and Actuators A: Physical*, 274:231–243, May 2018.
- [15] Yanan Wang and Xiang Li. 4d printing reversible actuator with strain self-sensing function via structural design. *Composites Part B: Engineering*, 211:108644, April 2021.
- [16] Xue Wan, Yang He, Yanju Liu, and Jinsong Leng. 4d printing of multiple shape memory polymer and nanocomposites with biocompatible, programmable and selectively actuated properties. *Additive Manufacturing*, 53:102689, May 2022.
- [17] Qi Ge, Amir Hosein Sakhaei, Howon Lee, Conner K. Dunn, Nicholas X. Fang, and Martin L. Dunn. Multimaterial 4d printing with tailorabile shape memory polymers. *Scientific Reports*, 6(1), August 2016.
- [18] Andreas Björnsson, Marie Jonsson, and Kerstin Johansen. Automated material handling in composite manufacturing using pick-and-place systems – a review. *Robotics and Computer-Integrated Manufacturing*, 51:222–229, June 2018.
- [19] E3D-Online. Toolchanger and motion system bundle, 2022.
- [20] E3D-Online. E3d hemera direct kit (1.75mm), 2022.
- [21] Sparkfun. Uhf rfid tags - adhesive, 2022.
- [22] Sparkfun. ua7800 series positive-voltage regulators, 2022.
- [23] William Makinen. Cos 598 final project videos, 2022. Available at [https://drive.google.com/drive/folders/1FURgstYYWmrUtmOymRtRT9fdZl\\_3dFqz?usp=share\\_link](https://drive.google.com/drive/folders/1FURgstYYWmrUtmOymRtRT9fdZl_3dFqz?usp=share_link).
- [24] Jacques Cali, Dan A. Calian, Cristina Amati, Rebecca Kleinberger, Anthony Steed, Jan Kautz, and Tim Weyrich. 3d-printing of non-assembly, articulated models. *ACM Transactions on Graphics*, 31(6):1–8, November 2012.

- [25] Duet3D. Reprappingfirmware 3 overview, 2022.
- [26] ISO. ISO 6983-1:1982 —numerical control of machines — program format and definition of address words — part 1: Data format for positioning, line motion and contouring control systems, 2022.
- [27] Andrew Gleadall. FullControl GCode designer: Open-source software for unconstrained design in additive manufacturing. *Additive Manufacturing*, 46:102109, October 2021.
- [28] Sunpreet Singh, Gurinder Singh, Chander Prakash, and Seeram Ramakrishna. Current status and future directions of fused filament fabrication. *Journal of Manufacturing Processes*, 55:288–306, July 2020.
- [29] William C Stone. NIST construction automation program, report no. 3:. Technical report, 1997.
- [30] Sparkfun. Sparkfun simultaneous rfid reader - m6e nano, 2022.
- [31] Arduino. What is arduino?, 2022.
- [32] Hyginus E. Opara, Uchechi G. Eziefula, and Bennett I. Eziefula. Comparison of physical and mechanical properties of river sand concrete with quarry dust concrete. *Selected Scientific Papers - Journal of Civil Engineering*, 13(s1):127–134, March 2018.
- [33] Roland J.-M. Pellenq and Henri Van Damme. Why does concrete set?: The nature of cohesion forces in hardened cement-based materials. *MRS Bulletin*, 29(5):319–323, May 2004.
- [34] Practice for making and curing concrete test specimens in the field.
- [35] Pratiksha Andhare and Sayali Rawat. Pick and place industrial robot controller with computer vision. In *2016 International Conference on Computing Communication Control and automation (ICCUBEA)*. IEEE, August 2016.